ADVANCED OPTICAL MATERIALS
www.advopticalmat.de

Laser Photochemical Nanostructuring of Silicon for Surface Enhanced Raman Spectroscopy

*Alp Akbıyık, Nardin Avishan, Özge Demirtaş, Ahmet Kemal Demir, Emre Yüce, and Alpan Bek**

In this work, a novel method of fabricating large-area, low-cost surface-enhanced Raman spectroscopy (SERS) substrates is explained which yields nanostructured surface utilizing laser-induced chemical etching of crystalline silicon (Si) in an hydrofluoric acid solution. Nanostructuring of Si surface is followed by deposition of a thin noble metal layer to complete the fabrication procedure. A 50 nm thick silver (Ag) layer is shown to maximize the SERS performance. The SERS effect is attributed to the electromagnetic field enhancement originating from the nanoscale surface roughness of Si that can be controlled by the illumination power, etch duration, and the spot size of the laser beam. The SERS substrates are found to be capable of detecting a Raman analyte dye molecule down to 10^{-11} M. SERS performance of the Ag deposited substrates are compared to gold (Au) deposited substrates at 660 and 532 nm excitation. Nanostructured Si surface with Ag exhibits stronger SERS than with Au under 532 nm excitation exhibiting an enhancement factor as high as 10^9. Raman enhancement factor is calculated both by SERS spectra experimentally, and using finite-elements simulation of the electric field enhancement. The applicability of the fabricated substrates is examined by adsorbing different analytes.

1. Introduction

Photochemical (PC) etching and surface texturing of silicon (Si) have been attracting the attention of the nanotechnology and materials science community for more than several decades owing to its potential for facile, large area, and single-step surface structuring capability at the nanoscale. Although basic scientific studies of photochemically nanostructured Si have been conducted extensively, there has been slow progress in the development of applications utilizing the nanotextured Si surface as an optical material. Only recently, the PC etching method along with its cousins, photoelectrochemical and electrochemical etching, has been revisited and the resulting surface nanostructures have been systematically and comparatively studied.[1] Here, we report on novel surface-enhanced Raman spectroscopy (SERS) substrates that utilize photochemical etching of Si in creating a nanoscale texture of its surface especially suitable to host electromagnetic hot-spots over extended areas followed by a simple noble metal evaporation step. The advances in nano-scale physics and material science that utilize plasmonic resonance enhancement via noble metals brought the concept of SERS to the forefront.[2,3] SERS substrate fabrication methods and configurations have constantly advanced since then. Moreover, numerous applications in the field of material science, biology, chemistry, and the food industry keep SERS as an increasingly influential technique.[4] There are numerous fabrication methods to enhance the Raman signal of a substance in the literature. Raman enhancement can be mainly achieved either by chemically changing the polarization due to charge transfers with the molecule or by creating electromagnetic hot-spots on the surface of a substrate.[5,6] The latter phenomenon, namely, near field electromagnetic enhancement, requires nanostructures made of noble metals such as silver (Ag) and gold (Au), along with their alternatives such as copper (Cu) and aluminum (Al).[7] It provides the most powerful Raman signal enhancement through the hot-spots formed among the structures. The synthesis and fabrication methods of plasmonic nanostructures are widely studied in the literature. For a SERS substrate, there are many nanostructure configurations through which electromagnetic field can be enhanced. This enhancement varies throughout the surface morphology even in the same material.[8–10] A significant portion of these substrate structures rely on embedding plasmonic nanoparticles on a substrate to enhance the signal within the hot spots.[3] Si surface structuring techniques are functional and more convenient when the surface morphology significantly contributes to the desired application. Micro and nanostructuring methods are

A. Akbıyık, E. Yüce, A. Bek
Physics Department
Middle East Technical University
Ankara 06800, Turkey
E-mail: bek@metu.edu.tr
N. Avishan, Ö. Demirtaş, E. Yüce, A. Bek
Micro and Nanotechnology Program
Middle East Technical University
Ankara 06800, Turkey
A. K. Demir
Physics Department
Bilkent University
Ankara 06800, Turkey
The ORCID identification number(s) for the author(s) of this article can be found under https://doi.org/10.1002/adom.202200114.

DOI: 10.1002/adom.202200114

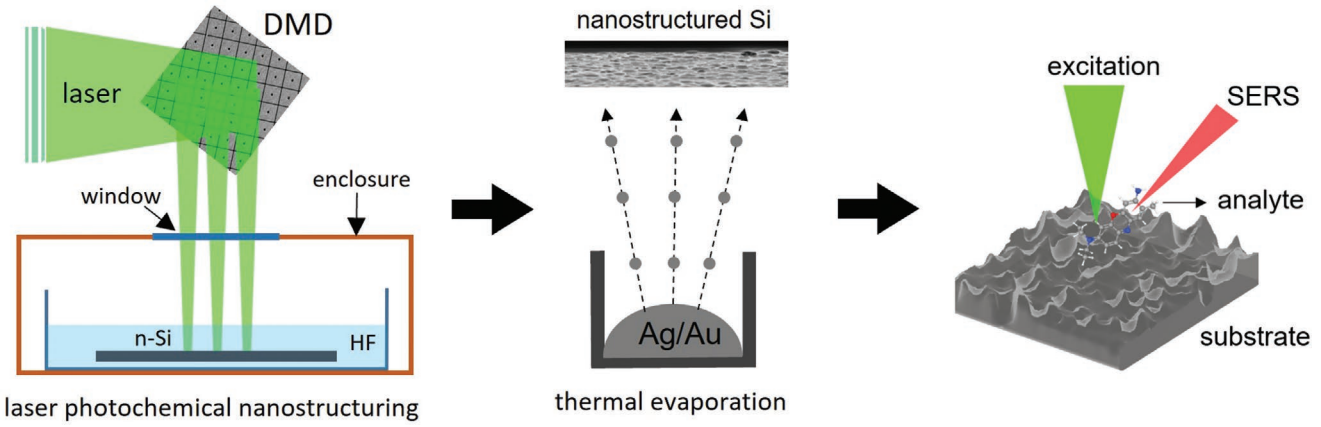

Figure 1. Two-step fabrication of novel SERS substrates from left to right: laser photochemical nanostructuring of Si surface followed by thermal evaporation of Ag/Au and assessment of its SERS potential using a Raman reporter molecule.

used in several applications like sensing, anti-reflection coatings in photovoltaics, SERS substrates, and so on.[11] Crystalline Si surface can be structured in many ways; directly by pulsed laser, plasma, and wet etching. These periodic,[12,13] porous,[14–16] or black Si structures are also structured with synthesized plasmonic nanoparticles,[17] however; those substrates may suffer from the non-uniformity of the localized surface plasmon resonance (LSPR) along the surface. Even with the uniform coating and strong hot-spots, ion-beam lithography techniques suffer from the fabrication costs, time, and small area.[18]

In this work, we demonstrate that the method of laser-assisted PC etching,[19–23] where the etching reaction of hole generation is ignited by laser illumination instead of electrodes or metal,[24–27] can effectively be used to fabricate highly field enhancing macroscopically large area SERS substrates with 10 picomolar limit-of-detection (LoD) at a low cost. The laser illumination is spatially shaped and controlled using a digital micro-mirror device (DMD). The implementation of DMD in laser-assisted chemical etching, which we introduce here, enables precise and adaptive control of the laser beam. The laser beam size and illumination power on the sample are precisely modified without the need to change optics for different structures. Moreover, the scheme that we introduce, enables us to creation of advanced and functional patterns without scanning the laser beam during the fabrication process.

Using the spatially shaped laser-assisted chemical etching method, nanoholes are created on the surface of the Si. When combined with a metallic thin film, for example, Ag coating on top of the etched surface, the substrate provides local field enhancement that increases Raman signal essentially by the abundance of the gap plasmon modes. The thin film deposited SERS substrates can also be composed of periodically structured surfaces.[28] Compared to such structures such as gratings and cavities fabricated via photolithography or direct laser structuring,[29] the nanoholes in our rough Si samples are more randomly distributed on the surface. This enables us to expect further morphology-dependent enhancement apart from the metallic film features. Even in the deepest etched structure, hole depths do not exceed nanoscale dimensions and the roughness still remains shallow unlike SERS substrates with black Si structures[30] fabricated by metal-assisted etching or reactive-ion etching (RIE).[31,32] The general schematic view of each step toward the fabrication of the substrate is shown in **Figure 1**. The nanostructured surfaces are fabricated by PC etching of Si wafer and controlled thickness of Ag and Au are deposited on these structures by thermal evaporation. Brilliant cresyl blue (BCB), one of the most popular tracer dyes, is used as the analyte molecule to check the SERS response. Then, a relative EF is calculated by acquiring SERS spectra of BCB adsorbed on Ag and Au deposition following photochemically structured Si surfaces as compared to the bare Si.

2. Results and Discussion

2.1. Effect of Metal Film Thickness on SERS Enhancement

Comparative study regarding the effect of Ag thickness on the SERS enhancement mechanism is reported by keeping the laser-assisted wet etching parameters constant. The maximum SERS signal is obtained for Ag coating thickness values between 40–60 nm as shown in **Figure 2**a,b. Below and above these thickness values, the effect of plasmonic resonance on field enhancement starts to decrease. These optimum metal thickness values are certainly related to the depth of nanoholes, that is, the topography of Si surface after PC nanostructuring. On the one hand, as the average hole depth is in the 100 nm order, thicker than 100 nm Ag coating results in the fully covered surface and the hot-spots are mostly eradicated due to planarization. On the other hand, at less than 40 nm thickness, Ag is deposited non-uniformly throughout the rough surface, which results in a weak Raman enhancement due to large gaps and weaker gap plasmon intensities. It is found that a significant Raman enhancement is achieved for the substrates coated with 50 nm thick Ag, laser-assisted PC etch at around 200 mW illumination power, 15 min of etch duration, where the characteristic Raman peaks of BCB are observed down to 10^{-11} M as shown in Figure 2c. When combined in logarithmic scale in Figure 2d, intensity values of the brightest peak from consecutive BCB concentrations fitted with a linear curve until the lowest discernible Raman signal threshold, indicates 10^{-11} M as the LoD for BCB.

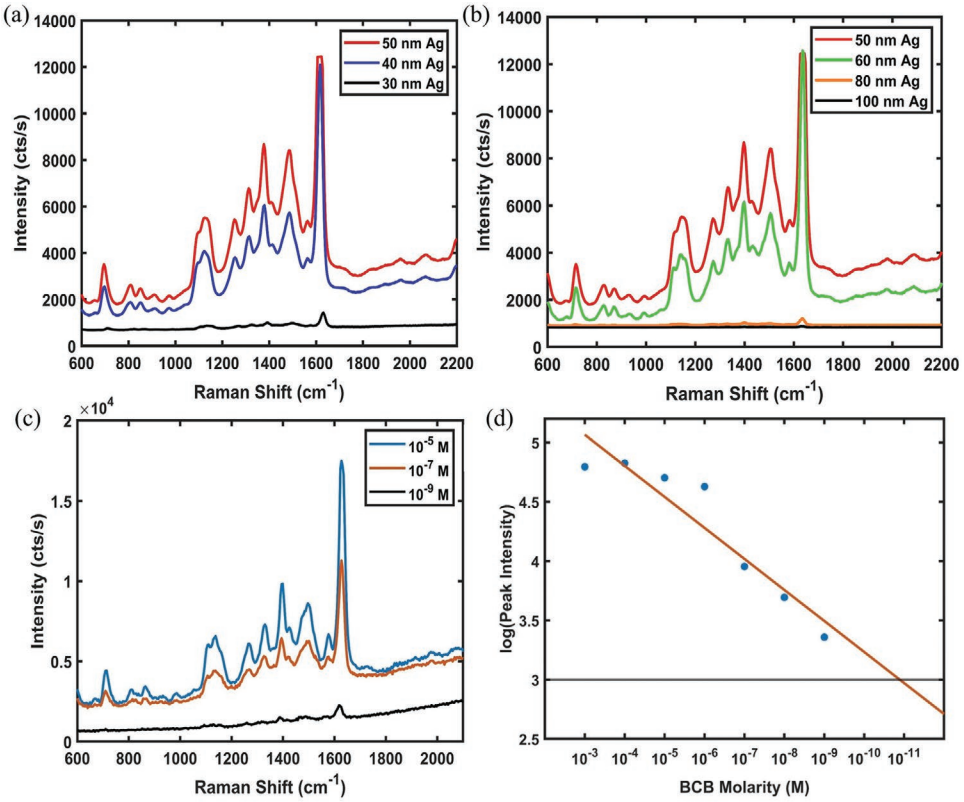

Figure 2. a) Ag deposition thickness impact on SERS signal varying from 30 up to 50 nm. b) Ag deposition thickness impact on SERS signal up to 100 nm. c) Raman spectra obtained at different BCB concentrations adsorbed on 50 nm Ag deposited substrates under 532 nm excitation. d) Determination of LoD from log(Raman signal) versus log(concentration) curve with a linear fit, horizontal line indicates the lowest discernible signal intensity of the Raman spectra.

SERS performance of the Ag deposited structures is also compared with the 50 nm Au deposited substrate as shown in **Figure 3**a,b. Au film is also deposited onto the PC etched Si surfaces with the same parameters. Ag deposited structure is observed to enhance the analyte molecule more than Au deposited structures under both 532 and 660 nm excitations. Different Raman excitation wavelength performances are shown in Figure 3a,b for 50 nm Au and Ag substrates, respectively. Although one might expect different enhancement performance with changing plasmonic material and excitation wavelength, the substrate topography is a crucial factor here for SERS enhancement as will be revisited in later sections.

2.2. Effect of Surface Nanostructuring on SERS Enhancement

In the same Ag thickness, most enhanced Raman signals are observed from the substrates with dense etched surfaces and no significant signal is obtained from Ag on a flat Si surfaces. In the Raman map shown in **Figure 4**a, 50 nm Ag deposited

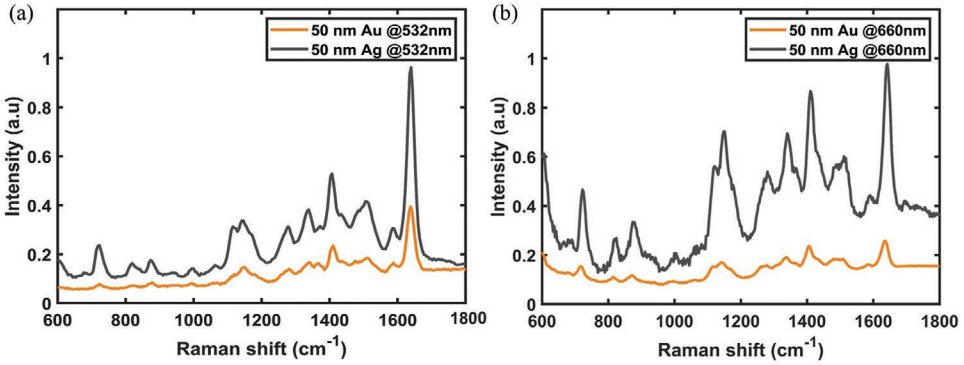

Figure 3. SERS spectra of both 50 nm deposited and 10^{-5} M BCB adsorbed Ag and Au substrates under a) 532 nm and b) 660 nm laser excitation.

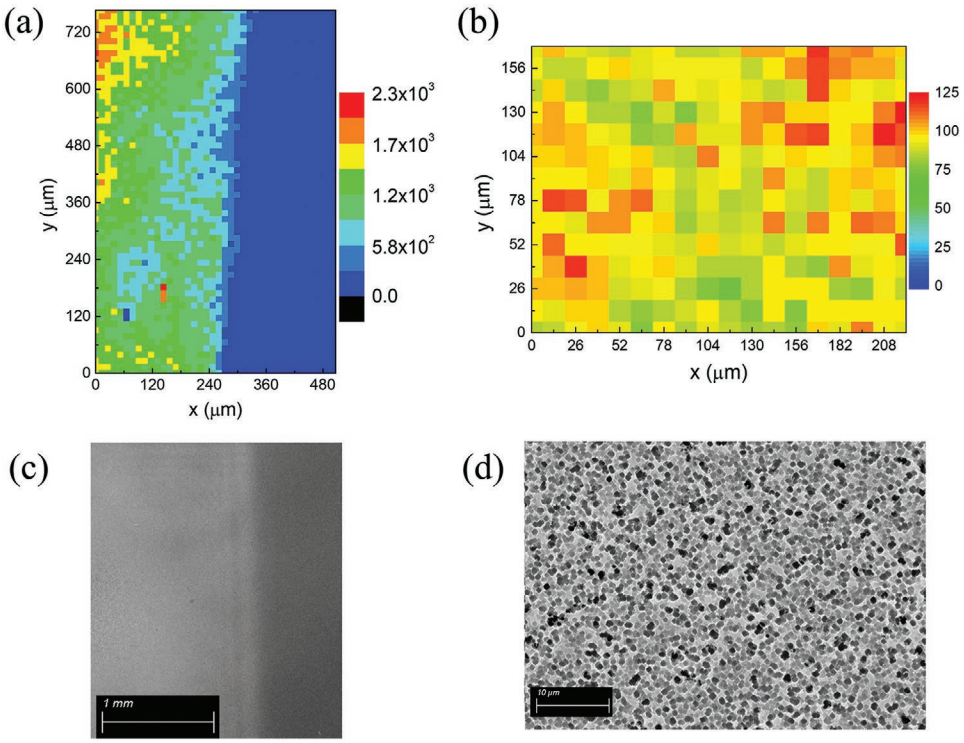

Figure 4. Raman map of 50 nm Ag deposited and 10^{-5} M BCB coated on substrates showing a) the effect of field enhancement in the transition region between illuminated and non-illuminated area, b) signal variation of SERS intensity related to structured part-Raman maps obtained by 532 nm excitation wavelength and analysis of 573 cm^{-1} Raman band of BCB. SEM images showing c) the transition from structured to non-structured part and d) structured part with higher magnification.

substrate is scanned over the transition region between illuminated and non-illuminated area. SERS signals notably diminish as the nanohole density decreases across the pattern border. Blue part corresponds to the Ag deposited on less structured Si surface. Details of the mapping can be found in Figure S1, Supporting Information. On the other hand, also merged and wider nanoholes formed by strong etching tend to decrease the field enhancement due to weakened hot spots. It is shown that the best SERS performance can be achieved by adjusting the appropriate illumination power, etch duration, and HF/oxidant concentration in the solution.[31] The homogeneity of the SERS activity of Si surface structuring followed by spin coating of 10^{-5} M BCB solution has been investigated by Raman mapping as shown in Figure 4b, revealing a ±26% variation of the SERS intensity over a 3.73×10^{-2} mm^2 area. Figure 4c,d, shows SEM images of the transition from structured to non-structured part and only structured part with higher magnification, respectively.

The bar graphs in **Figure 5** show the effect of laser power, duration of laser illumination, and the beam spot size on the SERS signals from the substrates fabricated with such parameters. In the Raman measurements from these substrates, Ag thickness is kept at 50 nm and the BCB concentration is 10^{-5} M for all the samples. The beam spot size is adjusted merely by DMD by keeping the laser output power constant. The reason for the Raman signal drop due to smaller spot size is that as the laser intensity goes higher with decreasing beam area, etched holes on the Si surface become larger and reach the micron scale. Thus, as mentioned above, merging or widening of the holes diminish the electromagnetic field enhancement coming from the hot-spots. Corresponding changes in the nano-holes can be observed from the microscope images in the Figure S2, Supporting Information, with varying spot sizes. As a result, we find that the optimal SERS enhancement is obtained from

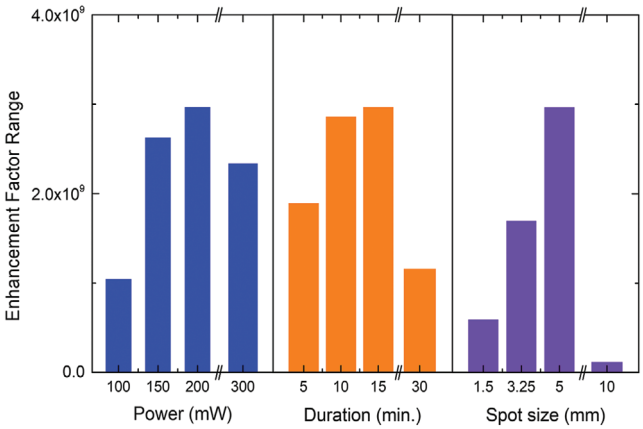

Figure 5. Comparison of the EF values using the characteristic peak at 1653 cm^{-1} acquired from 10^{-5} M BCB adsorbed on different substrates fabricated by various Si etching parameters keeping the Ag thickness constant at 50 nm. The left panel shows the substrates etched at different laser powers (same spot size), the central panel shows the substrates etched with different duration at the same laser power, and the right panel shows the substrates etched at different spot sizes.

Table 1. SERS enhancement factors of substrates fabricated using various illumination dependent and metal thickness parameters.

Substrate	Etching parameters	Deposition	EF
1	200 mW – 15 min	50 nm Ag	2.91×10^9
2	200 mW – 15 min	30 nm Ag	3.50×10^8
3	100 mW – 15 min	50 nm Ag	1.02×10^9
4	200 mW – 5 min	50 nm Ag	1.89×10^9
5	200 mW – 15 min	80 nm Ag	8.73×10^7
6	200 mW – 15 min	50 nm Au	5.24×10^8

the substrate nanostructured with a 200 mW laser power and 5 mm beam size in 15 min.

2.3. Evaluation of SERS Performance and Comparison with Theory

Enhancement factor calculation is conducted based on the characteristic peak areas indicated as Raman and SERS intensity in Equation (1). Here, the calculated peak around 1653 cm^{-1} is assigned to the Raman band of symmetrical in-plane C–C stretching.[33] The enhancement factor calculation uses the notion of the number of the adsorbed analyte molecule indicated as N_{Raman} and N_{SERS}.[3] In **Table 1**, calculated approximate EF values of various substrates are based on the reference BCB measurements of 10^{-2} M as N_{Raman} and I_{Raman}. In normal Raman spectroscopy (NRS) inside liquid samples, the 3D Raman probe volume can be determined by considering a prolate spheroid focal volume, which in our case have dimensions of r_x = 8.5 µm, r_y = 8.5 µm and the depth of focus r_z = 17 µm, yielding $V_{probe} = \left(\frac{4\pi}{3}\right) \times 8.5\,\mu m \times 8.5\,\mu m \times 17\,\mu m = 5144.88\,\mu m^3 = 5.14 \times 10^{-12}\,L$ of probe volume. For our 10^{-2} M BCB solution, the total number of molecules, namely, $N_{NRS} = C_{NRS} \times V_{probe}$, in the measurement volume can be found as $N_{NRS} = 10^{-2} mol\,L^{-1} \times 6.02 \times 10^{23}$ molecules $mol^{-1} \times 5.14 \times 10^{-12} L = 3.09 \times 10^{10}$ molecules. After baseline correction, I_{NRS} is calculated through the area under the characteristic peak 1653 cm^{-1} is found as 2500 cts s^{-1}. The surface area of the structures obtained from COMSOL simulation environment is 281.31 μm^2. Molecules in the near field enlarge up to 2 nm from the surface of the metal film, we deliberately exaggerate this value as 5 nm in order not to to overestimate the EF value, resulting in a probe volume of V_{probe} = 281.31 $\mu m^2 \times$ 0.005 µm = 1.41×10^{-15}L. Therefore, the total number of BCB molecules in the SERS measurement can be calculated as $N_{SERS} = 10^{-5} mol\,L^{-1} \times 6.02 \times 10^{23}$ molecules $mol^{-1} \times 1.41 \times 10^{-15} L =$ 8.49×10^3 molecules. The EF is calculated with the measured I_{NRS} and I_{SERS} values as $EF = \frac{I_{SERS}}{2500} \times \frac{3.09 \times 10^{10}}{8.49 \times 10^3}$.

In order to complement the Raman results, we also study the expected far-field contribution of the Ag and Au substrates based on their scattering spectra obtained from both dark-field spectroscopy measurements and finite-difference time-domain (FDTD) simulations based on a simple model of the substrates. Experimental dark-field scattering spectra and FDTD simulated spectra are given in **Figure 6**a,b. **Table 2** indicates the values of both excitation wavelengths, 532 and 660 nm, and corresponding Raman shifted values of 1653 cm^{-1} BCB peak. According to the calculations from the experimental dark-field scattering data, enhancement improvement EI ≈2.7 for 532 nm excitation and EI≈1.6 for 660 nm. This means Ag deposition has improved the enhancement almost 3 times in 532 nm and 1.6 times in 660 nm over Au deposition. Experimental dark field scattering spectra show the far-field picture while the scattering cross-section obtained from FDTD simulations mostly shows the near-field picture. The trend for Au and Ag substrate of the same thickness and etching parameters remains similar, which underlines the effect of nano-hole size and shape in addition to the used material. For larger and complex nanostructure geometries, scattering response dominates the extinction spectra and such structures exhibit richer Mie features rather than a single dipole-like Rayleigh peak. Our photochemical Si nanostructuring technique reproducibly yields structures when coated with Ag exhibit significantly higher enhancement than when coated with Au under both 532 and 660 nm excitations. The difference between EF factors from dark-field and SERS is worth mentioning. As pointed out above, dark-field spectra show the far-field response. So, it can be concluded that the enhancement factors partially originate from shape-dependent plasmon resonances[34] that are supported by

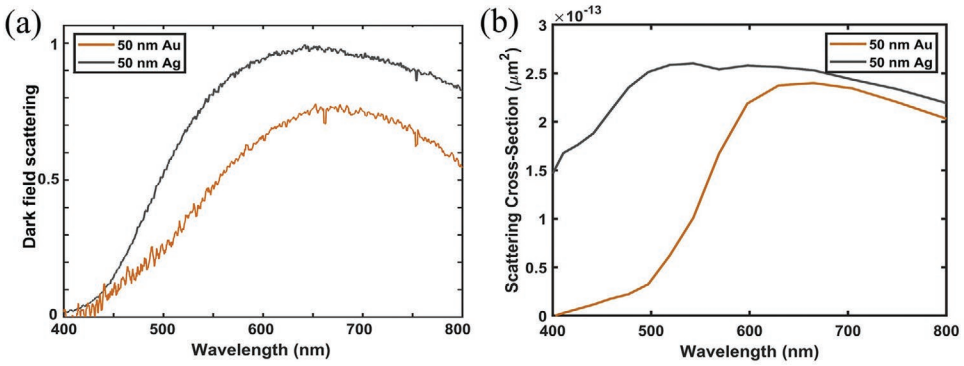

Figure 6. a) Normalized scattering spectra of the 50 nm deposited Au and Ag substrates on Si nanoholes obtained via dark field scattering. b) Scattering cross-sections calculated using FDTD simulations.

Table 2. Normalized intensity values obtained from both dark field scattering spectra and simple FDTD simulation model scattering cross-section of 50 nm deposited Ag and Au substrates. Corresponding I_{Raman} values are found from the corresponding wavelength positions of the Raman shifted BCB peak around 1653 cm^{-1}. Total here denotes the product of the intensities calculated from the normalized scattering data.

	Dark field spectrum			FDTD		
Substrate	$I_{excitation}$ (532 nm)	I_{Raman} (582 nm)	Total	$I_{excitation}$ (660 nm)	I_{Raman} (738 nm)	Total
50 nm Ag on Si	0.73	0.91	0.66	0.98	0.93	0.91
50 nm Au on Si	0.38	0.63	0.24	0.76	0.71	0.54

the nanostructured substrate morphology, in addition to the material resonances.

$$EF = \frac{I_{SERS}}{I_{Raman}} \times \frac{N_{Raman}}{N_{SERS}} \quad (1)$$

For a better understanding of the fabricated structure and enhancement mechanism due to geometry, a detailed finite-element methods (FEM)[35] simulation model of the photochemically structured morphology is also shown in **Figure 7** based on the cross-sectional image of the substrate. Simulation details can be found in Supporting Information. In order to compare the field enhancement with Raman spectra and dark-field spectra in a numerical sense, the simulated enhancement factor is calculated according to electric field distribution around the structure. Based on the FEM simulations of electric field distribution as mapped in Figure 7, enhancement factor is calculated using the approximation of $EF = |E/E_0|^4$. FEM calculations yield numerical EF values reaching up to 10^9 and 10^8 under 532 and 660 nm excitations, respectively, at the hot-spots created in the roughened surface which agree very well with the experimentally determined EF values as shown in Figure 5. It is noteworthy to observe that the numerical model being faithful to the SEM image belonging to such a rough surface is successful to provide realistic trends of enhancement factors. We think that remaining as faithful as possible to the actual detailed surface geometry as acquired from SEM/AFM images rather than simplifying it to a combination of circles, triangles, and rectangles as an often adopted practice, may be a key factor in designing and optimizing substrates for particular excitation wavelengths.

Other prominent factors besides enhancement factor that define the quality of the SERS substrates are reproducibility, uniformity, and reliability. Consistency of the signals among the substrates with the same parameters is the indicator of a reproducible and uniform substrate. From the Raman mappings in the Figure S3, Supporting Information, uniform signals can be observed from the substrates fabricated under the same conditions. Furthermore, it is the variety of analyte molecules examined that make a SERS substrate useful. Thus, we present the evaluation of the fabricated SERS substrates for those mentioned factors, either. In **Figure 8** we show the applicability of the same substrates for different analyte molecules by adsorbing Rhodamine 6G (R6G), Crystal Violet (CV), and ammonium nitrate (NH_4NO_3). These few-weeks old substrates deposited with 50 nm Ag show decent and significantly enhanced signal for the corresponding molarities compared to normal Raman spectra of the same molecules. R6G and CV are commonly used dye molecules[36] whereas NH_4NO_3 is used as fertilizer and explosive material which bears significance for its detection. The observed Raman bands in Figure 8a,c are partially common with BCB spectra shown in above figures, for the wavenumbers around 1200, 1400, and 1600 cm^{-1} whereas in NH_4NO_3 characteristic peak is found at 1045 cm^{-1} denoting the N–O symmetric stretching.[37]

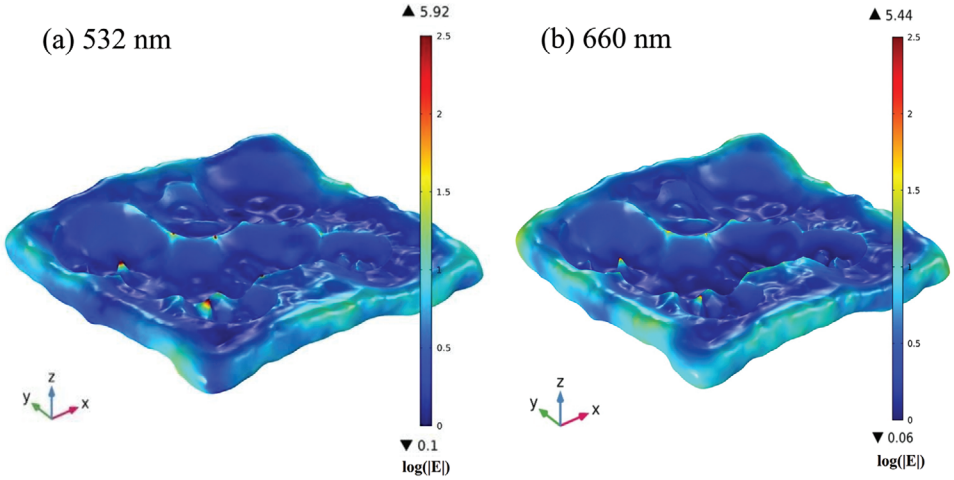

Figure 7. FEM simulation of the nanostructured 50 nm Ag substrate surface under both a) 532 and b) 660 nm illumination as used in SERS experiments using COMSOL. Color bars denote the electric field strength in logarithmic scale.

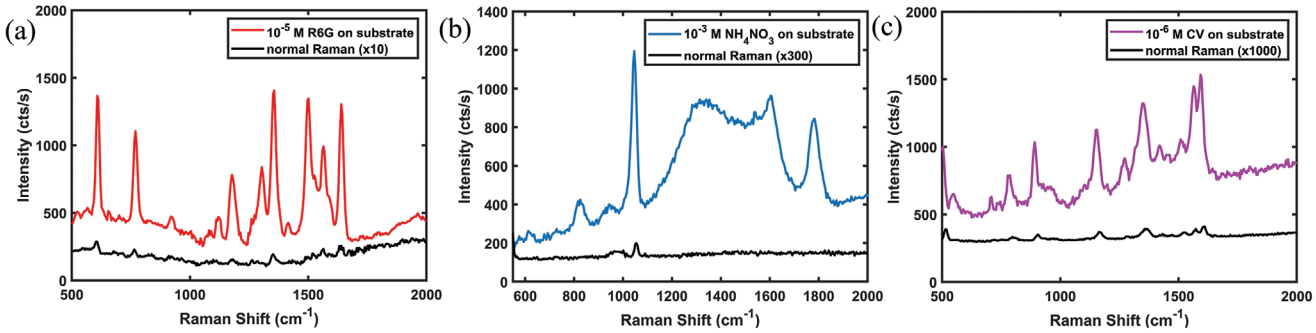

Figure 8. Raman spectra of a) 10^{-5} M R6G dye molecule, b) 10^{-3} M NH_4NO_3, and c) 10^{-6} M CV dye molecule under 532 nm excitation using substrates with the same structuring parameters and 50 nm Ag compared with their normal Raman spectra.

3. Conclusion

A significant enhancement of Raman scattering signal is obtained from the analyte molecule BCB using these fabricated substrates composed of the hot spots created via laser-assisted chemical etching of Si utilizing DMD. Furthermore, Si roughness and resulting SERS activity is shown to be greatly affected by illumination power, duration, and beam spot size by keeping the other parameters such as analyte concentration, Ag thickness, and the HF, oxidant concentrations in the solution constant. These mentioned roughness parameters affect SERS activity, since they alter the substrate topography and distribution of the nanoholes on the substrate and thus, create plasmonic hot-spots in accordance with the metallic thin film. The optimized deposition thickness of 50 nm Ag is determined in accordance with the depth of the Si structures, so that, the resulting Ag coating is still uniformly deposited by keeping the rough structure intact. We report EFs up to 10^9 with 50 nm Ag thickness which corresponds to 6.50×10^4 ng cm^{-2} of Ag deposited on photochemically structured Si surface, significantly small amount of Ag use in SERS substrate fabrication as compared to commercial SERS substrates, with 1.41×10^9 ng cm^{-2}.[38] Moreover, as mentioned in the results section, the use of DMD decreases the amount of fabrication time. Therefore, these substrates are cost-effective in terms of both fabrication costs and time. The fabricated structures with Ag are compared also with under 660 nm laser excitation and Au deposited substrates and the resulting spectra clearly show that 532 nm Raman excitation and Ag deposited morphology give better enhancement results, despite the stability of Au deposition. Further demonstration of the substrate performance is reported on different analyte molecules. Raman mappings are shown for uniformity among the substrates fabricated under the same conditions. Upcoming research is conducted for these structures in order to enhance their activity on many different analyte molecules under alternative laser excitations, metal/dielectric coatings, new surface morphologies, and tunable nanoparticle decorations.

4. Experimental Section

Surface Nanostructuring of Si: The initial step toward the fabrication of SERS substrates reported here is photochemical etching of Si immersed in HF solution container. On the surface of the illuminated area, the reaction was initiated by the photoexcitation of the Si-HF solution interface and nanostructures were formed as a result of the anodic dissolution of Si and cathodic reduction of hydrogen peroxide, which was the oxidant. The resulting nanoholes are shown in the SEM image in **Figure 9**a. The overall reaction occurs as follows[11,31]

$$Si + 2H_2O_2 + 6HF \rightarrow H_2SiF_6 + 4H_2O \quad (2)$$

Since the reaction was initiated by the laser excitation, the etched surface nanostructures highly depended on the laser power, illumination time, and the concentrations of water, oxidant, and HF in the solution. Si wafer type, dopant type, level and the illumination wavelength[39,40] also affect the etching process. However, in this study, those factors were kept the same for simplicity. As shown in the Si energy band diagram in Figure S4, Supporting Information, migration of the photo-induced holes through the HF–Si interface in n-type Si played an important role to initiate the chemical reaction at the surface. Due to upward band bending at the Si–HF interface, when the electrons are separated from valence band with photoexcitation, the resulting holes can move into the surface. Moreover, with the aid of an oxidizing agent such as H_2O_2, electrons can be completely removed without recombining with the holes.[23,41] With the laser-induced holes coming from Si–Si backbonds

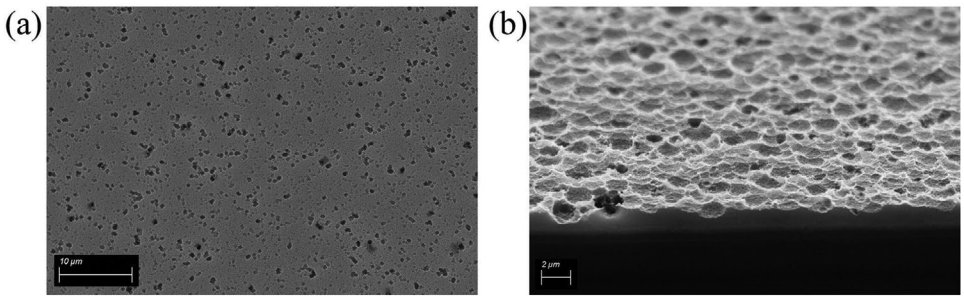

Figure 9. a) SEM image of photochemically etched Si surface. b) 50 nm Ag deposited rough Si surface that is the SERS substrate.

and having the dangling Si–F bond on the surface, nanostructure formation starts at the interface. Unlike n-type shown in Figure S4a, Supporting Information, there occurs no porosity on the illuminated area in p-type Si. Because laser-induced holes are carried away from the surface as shown in Figure S4b, Supporting Information.[1,23]

In the experimental setup for laser-assisted wet etching process shown in Figure 9, laser beam coming from the CW 532 nm light source was directed using the mirrors and lenses onto the micro-mirrors of DMD (Texas Instruments DLP6500 DMD, with resolution 1920 × 1080).[42] The spatial profile of the beam was controlled by the binary amplitude modulation provided by the DMD. Then, the shaped laser beam, for example, generated square patterns shown in Figure S5a,b, Supporting Information, was projected onto the container with the samples immersed in the HF solution. The beam shape and the spot size control through DMD ensured that a specific area of the Si wafer was etched more homogeneously, while the rest of the sample remained flat. A large area fabrication up to 1 cm^2 at one time was made possible owing to the flexibility of DMD. The comparison in reflectance spectra of fully and homogeneously etched Si surface and polished flat surface of Si is shown in Figure S6b, Supporting Information. In addition to the illuminated area, utilization of DMD was not limited to shaping of the beam spatially, it also provided duration control over the micro-mirrors. Thus, one can assign different exposure times to the incoming laser beam. The laser illumination process lasted between 5–15 min. Above 15 min and below 5 min, no significant hole formation was observed, in accordance with the HF and oxidant amount.

Deposition of Ag and Au via Thermal Evaporation: After the etching process, Ag was deposited via thermal evaporation technique onto the surface of the etched Si. Ag was deposited on the suitable thermal boats as pellets under 10^{-6} Torr pressure in 1 Å s^{-1} deposition rate. The substrates with Ag thickness from 30 nm up to 100 nm were fabricated in this study, while the depths of nanoholes on Si varied from 50 nm up to 200 nm with an average of 100 nm as characterized via AFM cross-section in Figure S6a, Supporting Information and individual nano-hole image in Figure S7, Supporting Information. The tilted SEM image in Figure 9b shows the fabricated SERS substrate with 50 nm deposited Ag. In order to compare with the Ag evaporated structures, Au film was also thermally deposited onto the likewise structured Si.

As an alternative approach to the thermal deposition of metals, a solution based approach was also tested for metal nanoparticle decoration of the laser nanostructured Si. The SERS study was conducted using 10^{-5} M BCB where the Raman spectra are provided in Figure S8, Supporting Information. Laser photochemical etched and flat Si samples were immersed in $AgNO_3$ solution for 3 and 5 min to form Ag nanoparticles. Below and above these durations, surface coverage either became too low or too high, not allowing for a conclusive study. It was found that although 5 min of immersion exhibited higher Raman enhancement over 3 min and laser irradiated parts exhibited higher Raman signals compared to non-irradiated ones as one would expect. Ag nanoparticle size and surface coverage needed a more detailed study for optimization of EF and uniformity.

Substrate Characterizations: As a final step, the Raman active molecule to be examined was spin coated onto the substrate composed of etched Si and thin film Ag. The dye molecule BCB was used as Raman active molecule on the substrates down to the 10^{-11} M dilution. Diluted aqueous solution of 0.05 mL BCB is spin coated at 1000 rpm for 1 min. Other dye molecules to be examined were also spin-coated in the same manner, whereas aqueous NH_4NO_3 solution was adsorbed by drop casting. Further details on the characterization techniques can be found in Supporting Information.

Supporting Information

Supporting Information is available from the Wiley Online Library or from the author.

Acknowledgements

Support from the Scientific and Technological Research Council of Turkey (TÜBİTAK) under grant nos. 119F101 and 118C24 is greatly acknowledged. A.A. thanks TÜBİTAK 2210E program and Ö.D. thanks TÜBİTAK 2211C program. The authors thank Prof. Ahmet Oral for giving access to the Raman spectrometer and the microscope, along with METU Central Laboratory and the operators for SEM and Raman map analysis.

Conflict of Interest

The authors declare no conflict of interest.

Data Availability Statement

The data that support the findings of this study are available from the corresponding author upon reasonable request.

Keywords

digital micro-mirror devices, etching, photochemistry, silicon, surface enhanced Raman spectroscopy

Received: January 17, 2022
Revised: April 7, 2022
Published online: May 29, 2022

[1] B. G. Rasheed, M. A. Ibrahem, *Micron* **2021**, *140*, 102958.
[2] S. Schlücker, *Chem. Int. Ed.* **2014**, *53*, 4756.
[3] J. Langer, D. Aberasturi, J. Aizpurua, R. A. Alvarez-Puebla, B. Auguié, J. J. Baumberg, G. C. Bazan, S. E. J. Bell, A. Boisen, A. G. Brolo, J. Choo, D. Cialla-May, V. Deckert, L. Fabris, K. Faulds, F. J. Abajo, R. Goodacre, D. Graham, A. J. Haes, C. L. Haynes, C. Huck, T. Itoh, M. Käll, J. Kneipp, N. A. Kotov, H. Kuang, E. C. Le Ru, H. K. Lee, Jian-Feng Li, X. Y. Ling, et al., *ACS Nano* **2020**, *14*, 28.
[4] S. Ben-Jaber, W. J. Peveler, R. Quesada-Cabrera, C. W. O. Sol, I. Papakonstantinou, I. P. Parkin, *Nanoscale* **2017**, *9*, 16459.
[5] M. Moskovits, *Phys. Chem. Chem. Phys.* **2013**, *15*, 5301.
[6] W. E. Doering, S. Nie, *J. Phys. Chem. B* **2002**, *106*, 311.
[7] R. D. Rodriguez, E. Sheremet, M. Nesterov, S. Moras, M. Rahaman, T. Weiss, M. Hietschold, D. R. T. Zahn, *Sens. Actuators, B* **2018**, *262*, 922.
[8] D. D. Evanoff, G. Chumanov, *Chem. Phys. Chem.* **2005**, *6*, 1221.
[9] S. L. Kleinman, R. R. Frontiera, A.-I. Henry, J. A. Dieringer, R. P. Van Duyne, *Phys. Chem. Chem. Phys.* **2013**, *15*, 21.
[10] R. J. C. Brown, M. J. T. Milton, *J. Raman Spectrosc.* **2008**, *39*, 1313.
[11] O. Volovlikova, S. Gavrilov, P. Lazarenko, *Micromachines* **2020**, *11*, 199.
[12] C. Zhang, S. Z. Jiang, Y. Y. Huo, A. H. Liu, S. C. Xu, X. Y. Liu, Z. C. Sun, Y. Y. Xu, Z. Li., B. Y. Man, *Opt. Express* **2015**, *23*, 24811.
[13] W. K. Hamoudi, A. M. Alwan, D. Sulaiman, *AIP Conf. Proc.* **2021**, *2372*, 080019.
[14] T. Ignat, R. Munoz, K. Irina, I. Obieta, M. Mihaela., M. Simion, M. Iovu, *Superlattices Microstruct.* **2009**, *46*, 451.
[15] M. Kosović, M. Balarin, M. Ivanda, V. Derek, M. Marciuš, M. Ristić, O. Gamulin, *Appl. Spectrosc.* **2015**, *69*, 1417.
[16] L. Mikac, M. Ivanda, M. Gotić, A. Maksimović, S. Trusso, C. D'Andrea, A. Foti, A. Irrera, B. Fazio, P. G. Gucciardi, *Croat. Chem. Acta* **2015**, *88*, 437.

[17] S. Chakraborti, R. N. Basu, S. K. Panda, *Plasmonics* **2018**, *13*, 1057.
[18] Q. Jiwei, L. Yudong, Y. Ming, W. Qiang, C. Zongqiang, W. Wudeng, L. Wenqiang, Y. Xuanyi, X. Jingjun, S. Qian, *Nanoscale Res. Lett.* **2013**, *8*, 437.
[19] L. Koker, K. W. Kolasinski, *Phys. Chem. Chem. Phys.* **2000**, *2*, 277.
[20] N. Noguchi, I. Suemune, *Appl. Phys. Lett.* **1993**, *62*, 1429.
[21] C. H. Choy, K. W. Cheah, *Appl. Phys. A* **1995**, *61*, 45.
[22] K. Kolasinski, *Encycl. Interfacial Chem.* **2018**, *2*, 611.
[23] K. Kolasinski, *J. Am. Chem. Soc.* **2013**, *135*, 11408.
[24] X. Yue, X. Zheng, G. Lv, J. Mo, X. Yu, J. Liu, Z. Jia, X. Iv, J. Tang, *Optik* **2019**, *192*, 162959.
[25] Y. Lai, J. Wang, T. He, S. Sun, *Anal. Lett.* **2014**, *47*, 833.
[26] A. A. Jabbar, A. M. Alwan, A. J. Haider, *Plasmonics* **2018**, *13*, 1171.
[27] H. Han, Z. Huang, W. Lee, *Nano Today* **2014**, *9*, 271.
[28] C. Lee, C. Robertson, A. Nguyen, M. Kahraman, S. Wachsmann-Hogiu, *Sci. Rep.* **2015**, *5*, 11644.
[29] L. Jinlong, J. Yang, S. Singh, Z. Zhan, Z. Yu, W. Xin, T. Huang, C. Guo, *Appl. Surf. Sci.* **2019**, *478*, 737.
[30] S. M. Asiala, J. M. Marr, G. Gervinskas, S. Juodkazis, Z. D. Schultz, *Phys. Chem. Chem. Phys.* **2015**, *17*, 30461.
[31] S. Bai, Y. Du, C. Wang, J. Wu, K. Sugioka, *Nanomaterials* **2019**, *9*, 1531.
[32] G. Gervinskas, G. Seniutinas, J. S. Hartley, S. Kandasamy, P. R. Stoddart, N. F. Fahim, S. Juodkazis, *Ann. Phys.* **2013**, *525*, 907.
[33] B. Bhushan, H. Fuchs, S. Kawata, *Applied Scanning Probe Methods V: Scanning Probe Microscopy Techniques*, Springer, Berlin **2006**.
[34] J. Zeng, F. Zhao, J. Qi, Y. Li, C. Li, Y. Yao, T. R. Leebc, W. Shih, *RSC Adv.* **2014**, *4*, 36682.
[35] Detailed Explanation of the Finite Element Method (FEM), https://www.comsol.com/multiphysics/finite-element-method (accessed: December 2021).
[36] J. Park, N. Oh, H. Nam, J. Park, S. Kim, J. S. Jeon, M. Yang, *Sensors* **2020**, *20*, 5089.
[37] N. M. Hadi, M. R. Mohammad. H. G. Abdulzahraa, *J. Al-Nahrain Univ.* **2017**, *20*, 60.
[38] M. E. Hankus, D. N. Stratis-Cullum, P. M. Pellegrino, in *Biosensing in Nanomedicine IV*, Vol. *8099* (Eds: H. Mohseni, M. H. Agahi, M. Razeghi), SPIE, Bellingham, WA **2011**, p. 80990N.
[39] M. Alwan, M. Salman, R. M. Shehab, *Indian J. Phys.* **2021**, *95*, 1843.
[40] M. Alwan, A. Yousif, A. Wali, *Plasmonics* **2018**, *13*, 1191.
[41] C. Cozzi, G. Polito, K. Kolasinski, G. Barillaro, *Adv. Funct. Mater.* **2017**, *27*, 1604310.
[42] D. Dudley, W. M. Duncan, J. Slaughter, *MOEMS Display and Imaging Systems*, Vol. *4985*, SPIE, Bellingham, WA **2003**, https://doi.org/10.1117/12.480761.